ISSN 0036-0244, Russian Journal of Physical Chemistry A, 2023, Vol. 97, No. 4, pp. 749–755. © Pleiades Publishing, Ltd., 2023.

PHYSICAL CHEMISTRY OF DISPERSED SYSTEMS AND SURFACE PHENOMENA

Optimization of Controlling Parameters of Porous Silicon Synthesis Using Taguchi Design of Experiment

Shivam Maurya[a,*], Sakti Prasanna Muduli[a,], Suman Nayak[b,***], and Paresh Kale[a,c,****]**

[a] *Department of Electrical Engineering, NIT Rourkela, Odisha, 769008 India*

[b] *Department of BioNest, Punjab University, Punjab, 160014 India*

[c] *DST-IIT Bombay Energy Storage Platform on Hydrogen, IIT Bombay, Maharashtra, 410076 India*

** e-mail: shivamckt123@gmail.com*

*** e-mail: pinkusakti08@gmail.com*

**** e-mail: sumannayak94@gmail.com*

***** e-mail: pareshkale@nitrkl.ac.in*

Received May 19, 2022; revised May 19, 2022; accepted July 7, 2022

Abstract—Porous silicon (PS) with high porosity is used in energy storage, solar photovoltaics, and sensing applications. The anodization method is the most widely used fabrication method since it is easy and economical. However, the method has various interdependent controlling parameters to fabricate PS, such as wafer resistivity, current density, hydrofluoric acid concentration, and anodization time. The parameters need to be optimized for a particular application to achieve the optimum porosity with fewer accouterments and time. The optimization can be carried out using the Taguchi design of experiment, which is based on the fractional factorial orthogonal array (OA). Mean output parameter graph, Signal to noise ratio, and interaction plot help to decide the interdependency and the optimized parameter for the desired output. The optimization achieved is validated by the factorial design of experiments.

Keywords: porosity, Taguchi design, orthogonal array, signal-to-noise ratio

DOI: 10.1134/S0036024423040295

1. INTRODUCTION

Porous silicon (PS)—a derived anisotropic and moreover homogeneous material from silicon—possesses tunable optical, physio-mechanical, and electronic properties such as porosity, surface area, refractive index, and bandgap, to list a few [1]. Engineering these properties via controlling the fabrication parameters led to the use of the free-standing PS film for various device and storage applications such as hydrogen storage, battery anode, sensors (bio and optical), solar photovoltaics, optics (e.g., waveguides), and due to its structures and dimensions of the pore [2–6]. Apart from formation parameters, PS properties can be tuned on surface modification of PS or implanting PS with foreign bodies such as enzymes [7] and metals [8].

Scores of methods reported in [9] to fabricate PS films can be categorized into two major groups based on the synthesis approach: top-down and bottom-up. The top-down procedure, such as ultrasonication [10], metallothermic reduction [11], and anodization, removes clusters of Silicon crystals from the substrate either chemically or physically. The bottom-up approach, such as microemulsion [12] and solution synthesis [13], arranges Si clusters to form bigger crystal structures, leaving space in between. Anodic etching or anodization is a widely used technique to form a porous layer on the surface of a silicon substrate [14]. Control over the porosity of the layer depends on the controlling parameters such as electrolyte concentration, the resistivity of the substrate, anodization time, and the anodization current. Porosity can be measured by the gravimetric method or by the Brunauer–Emmett–Teller (BET) technique directly [15]. The controlling parameter for the thickness of free-standing PS film is majorly the anodization time [16]. To optimize the morphology of the film, controlling parameters need to be optimized first. SEM micrographs can be used to determine pore size, pore size distribution, and film thickness.

The desired application governs the requirement of a particular property of the PS film. Since several parameters simultaneously affect the outcome, a set of parameters need to finalize to achieve an optimized structure for the application. Achieving the optimization of performing physical experiments, also known as the Factorial method, is a tedious and expensive stint considering the numerous possible combinations of parameters. To save the resources, the design of experiments (DOE) using optimization methods (e.g.,

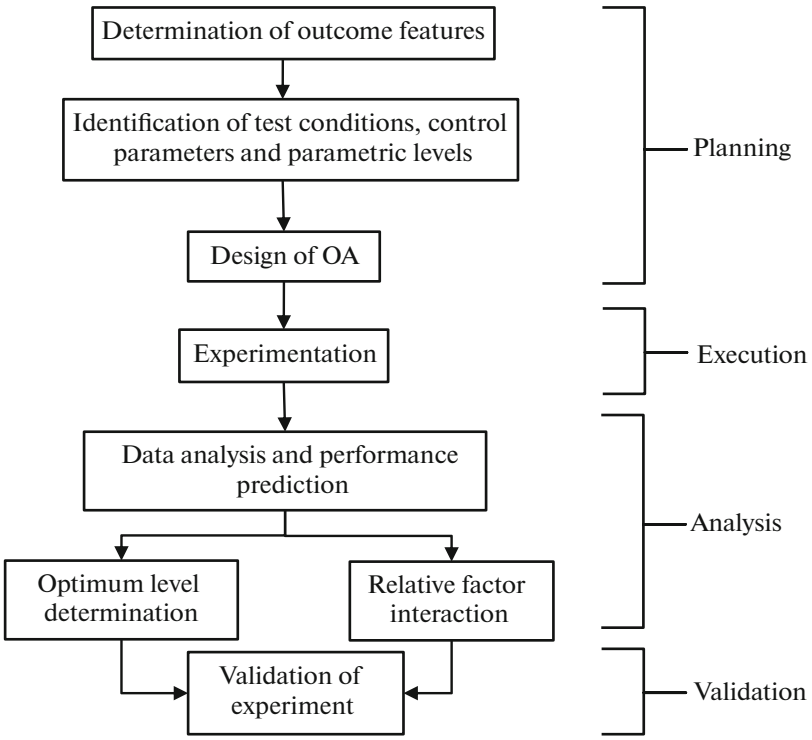

Fig. 1. Schematic flowchart of the porosity experimental design and procedure.

Response surface design, mixture design, optimal design, and Taguchi design) is an intelligent way out [17]. DOE studies the combined effect of controlling parameters variation having specific levels [18].

The Taguchi design is a statistical technique of optimization that uses fractional factorial design and orthogonal array (OA) [19]. The OA is the orthogonal matrix of fabrication parameters and parameter levels. A mixed OA is constructed if the parameter levels are different for the controlling parameters. The method helps design a minimum possible experiment using the OA to test the effect of the controlling parameters on the outcome. The first step is to construct the parameter matrix and prepare OA to carry out the Taguchi design. A reduced number of experiments with the controlling parameter combinations suggested by OA are then carried out, and the desired output parameters are measured. Using software like "Minitab 20.3.0," the data obtained is analyzed to calculate the signal-to-noise (S/N) ratio and interaction of parameters [20]. Either of three strategies decides optimization: larger-the-better (for maximization), smaller-the-better (for minimization), and nominal-the-best (for a particular fixed outcome or around the target). The algorithm to carry out the DOE using the Taguchi design is depicted in Fig. 1. The objective of the paper is to study the application of Taguchi Design to achieve optimal controlling parameters for PS fabrication for a particular application.

Table 1. Parameters and their levels employed in Taguchi design of experimental matrix (L18) for optimization of porosity parameters

Current, A	0.1	0.2	0.3	0.4	0.5	0.6
Levels	1	2	3	4	5	6
Resistivity, Ω cm	0.001–0.005		0.01–0.02		1–10	
Levels	1		2		3	
Electrolyte concentration	1 : 4		3 : 7		2 : 3	
Levels	1		2		3	

2. EXPERIMENTAL

Experimentation uses Silicon substrate (p-type and thickness ~250 ± 25 μm) with three different resistivities (0.001–0.005, 0.01–0.02, and 1–10 Ω cm) to form PS using the anodization method (refer to Fig. 2a) for various controlling parameters and levels as tabulated in Table 1.

The substrate is dipped into 40% HF for two minutes before anodization to remove native oxide formed on Si surface. The effect of HF concentration involves three different electrolyte concentration (HF to ethanol) ratios: 1 : 2, 3 : 7, and 2 : 3. The anodization current applied for 20 min and varied between 0.1 to 0.8 A

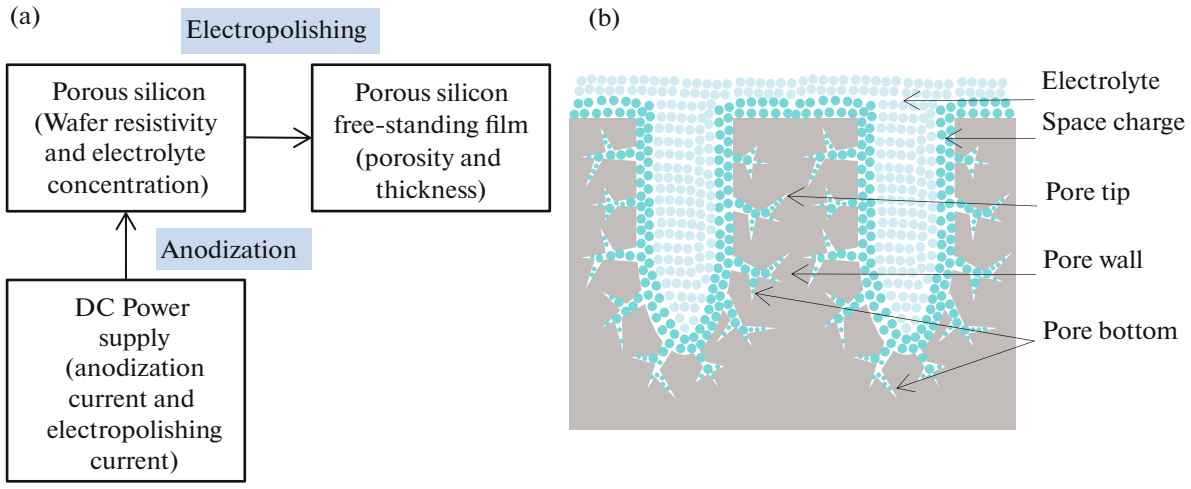

Fig. 2. Schematic of (a) fabrication porous silicon free-standing film, (b) pore and its terminology.

decides the level. Electropolishing at 2 A for one minute follows anodization, which lifts off the PS film using the two-step separation method. The porosity of the film is measured by gravimetric analysis. The porosity is maximized using a larger-the-better S/N ratio approach. S/N ratio is determined by Eq. (1), where n is the number of experiments and y_i is the response of each orthogonal array experiment [21]. Similarly, porosity can be minimized using a smaller-the-better S/N approach, where S/N is determined using Eq. (2)

Larger-the-better:

$$\frac{S}{N} = -10\log\left(\frac{1}{n}\sum_{i=1}^{n} y_i^2\right), \quad (1)$$

Smaller-the-better:

$$\frac{S}{N} = 10\log\left(\frac{1}{n}\sum_{i=1}^{n} y_i^2\right). \quad (2)$$

3. RESULTS AND DISCUSSION

When the anodization current increases, increased H^+ and F^- ions collide with the Si surface to increase the etching rate. The highly resistive wafer does not allow the low anodization current initially. However, as the pore grows gradually, the resistance decreases, allowing current to flow and increase porosity. The thickness and porosity of the PS film increase linearly with etching time. Due to prolonged chemical dissolution (anodization time), porosity and pore diameter increase.

The pore diameter and porosity decrease as the concentration of HF increases. The space charge layer width, which is decided by the anodization current and HF concentration, formed between the substrate and electrolyte, determines the pore size and wall thickness (refer to Fig. 2b). Due to the overlap of the two space charge regions at the entrance of adjacent pores, the substrate surface is depleted of carriers and is not conducting. When continued, it leads to pore collapse and merging. As a rule of thumb, if the pore wall thickness is more than twice the space charge layer width, it depletes the carriers, and etching continues horizontally. However, the pore formation continues vertically until the reaction is allowed to continue.

For a PS formed for controlled space charge layer width, the wall thickness is relative to the difference between the dissolution rate near the pore bottom (I_b) and the dissolution rate at the pore tip (I_t). If I_b is comparable to I_t, significant dissolution occurs near the pore bottom forwarding the vertical etching. Conversely, if I_b is small compared to I_t, the ions at the pore tip propagate relatively faster, promoting horizontal etching. The etching stops at the pore tip due to a lack of carriers; however, it is still ongoing at the pore bottom. Thus, the pore on the walls due to horizontal etching becomes smaller, making the pore wall between the adjacent pore thicker.

Figure 3a shows a Scanning Electron microscopic (SEM) image of PS film synthesized on p-type (0.01–0.02 Ω cm) with the anodizing current of 0.6 A, HF to the ethanol concentration ratio 2 : 3. The dependency of porosity on various controlling parameters is shown in Fig. 3b.

If the Full Factorial design is implemented, the total number of experiments required would be 54. This number reduces to 18 if the proposed Taguchi design is used for the number of levels of controlling parameters is considered.

Table 2 represents the orthogonal array matrix consisting of controlling parameter levels, the outcome as mean porosity, and the average S/N ratio. The Taguchi design is appropriate for an experiment with suffi-

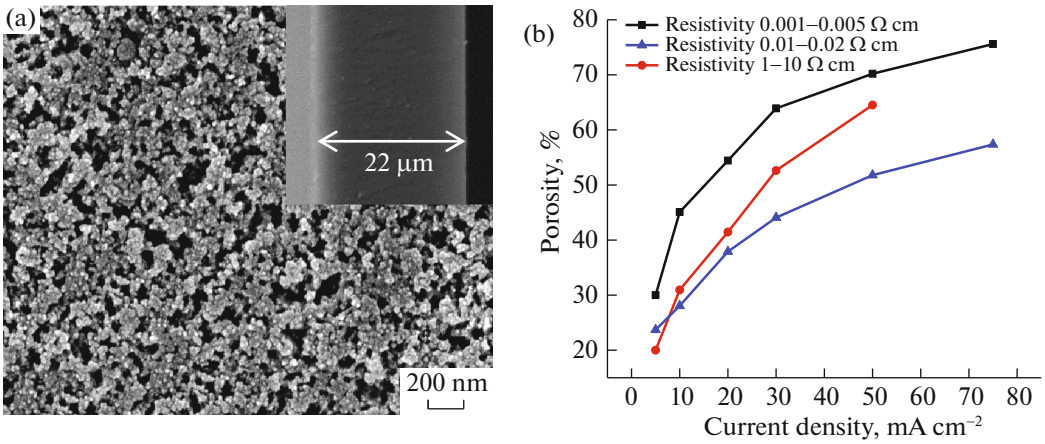

Fig. 3. (a) SEM image of the surface of PS synthesized by optimized parameters and cross-section image in the inset, (b) variation of porosity with current density for substrates of different resistivity and 1 : 4 electrolyte concentration ratio.

cient control parameters, enough levels, and multiple responses. If the controlling parameters for any experiment have different levels, an array cannot be formed for mixed design.

The pore morphology during the synthesis exhibits thin pore walls or the annihilation of walls. A well-accepted argument is that gravimetric analysis is not the best method to measure the porosity of the PS film. The errors shown by the method can be significant and unpredictable since the sources of errors are: moisture in the film and errors in the weights due to drying.

The mean porosity and S/N ratio graph at different anodization current, resistivity, and HF concentration levels are shown in Fig. 4. Suppose for an application; it is desired to maximize the porosity using a larger-the-better approach the set of controlling parameters would be anodization current of 0.4 A, substrate resistivity of 0.001–0.005 Ω cm, and 2 : 3 concentration

Table 2. Orthogonal array (L_{18}) of the Taguchi design for optimization of the controlling parameters

Experiment sequence	Controlling parameters			Output parameter	Mean S/N ratio, dB
	current, A	resistivity, Ω cm	concentration ratio	mean porosity, %	
L_1	0.1	0.001–0.005	1 : 4	64.92	36.25
L_2		0.01–0.02	3 : 7	15.76	23.95
L_3		1–10	2 : 3	77.67	37.81
L_4	0.2	0.001–0.005	1 : 4	70.67	36.98
L_5		0.01–0.02	3 : 7	29.82	29.49
L_6		1–10	2 : 3	73.90	37.37
L_7	0.3	0.001–0.005	3 : 7	51.44	34.23
L_8		0.01–0.02	2 : 3	27.98	28.94
L_9		1–10	1 : 4	36.15	31.16
L_{10}	0.4	0.001–0.005	2 : 3	70.94	37.01
L_{11}		0.01–0.02	1 : 4	33.82	30.58
L_{12}		1–10	3 : 7	89.11	38.99
L_{13}	0.6	0.001–0.005	3 : 7	50.84	34.12
L_{14}		0.01–0.02	2 : 3	36.92	31.35
L_{15}		1–10	1 : 4	52.60	34.42
L_{16}	0.8	0.001–0.005	2 : 3	72.95	37.26
L_{17}		0.01–0.02	1 : 4	41.37	32.33
L_{18}		1–10	3 : 7	43.85	32.84

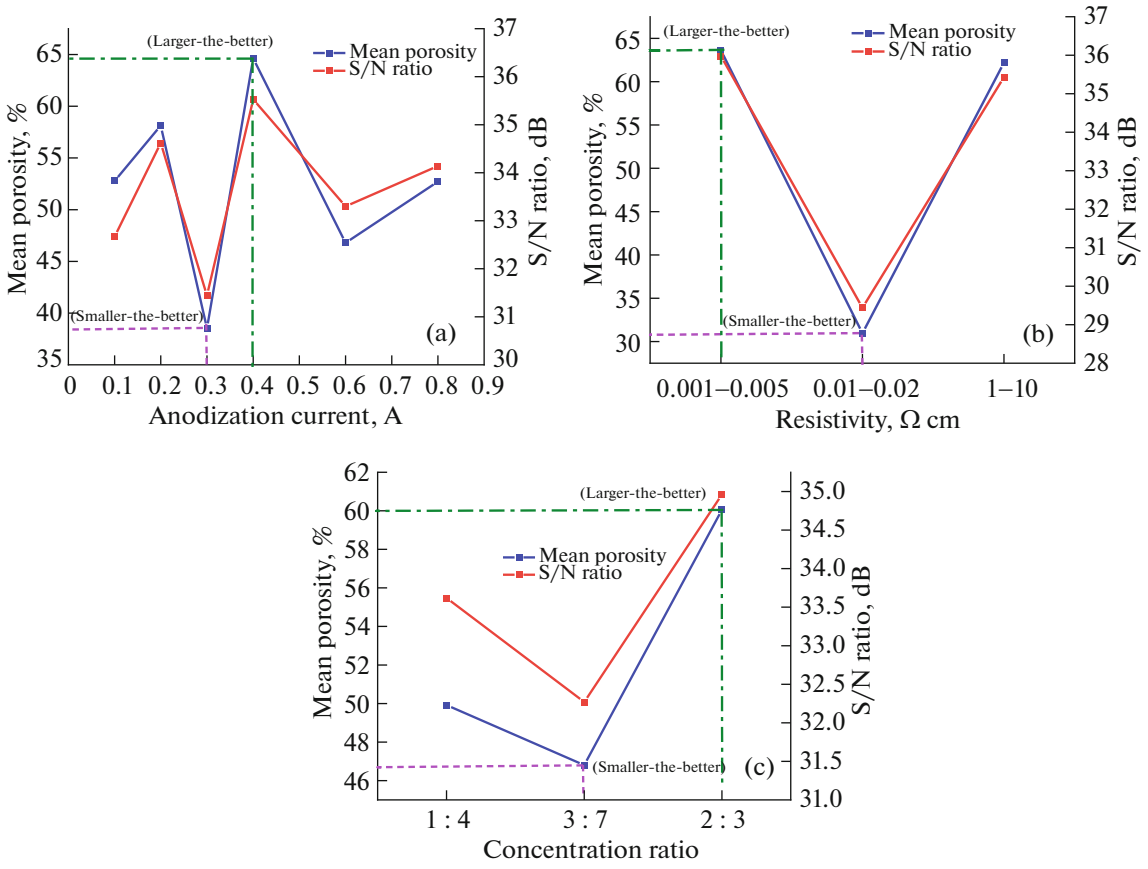

Fig. 4. The graph of mean porosity (%) and signal-to-noise (S/N) ratio at: (a) anodization current levels, (b) resistivity, and (c) HF and ethanol concentration ratio.

ratio (experiment sequence L_{10}). Whereas, if needed to minimize the porosity using a smaller-the-better approach, the optimized condition set would be the anodization current of 0.3 A, substrate resistivity of 0.01–0.02 Ω cm, and 2 : 3 concentration ratio (experiment sequence L_8). Though the combinations in experimental sequence L_3, L_6, L_{12}, and L_{16} result in mean porosity greater than L_{10}, the Taguchi design finalizes the L_{10} considering the effective mean of the porosity (refer to Fig. 4b). The effective mean of the porosity for resistivity ranges 0.001–0.005, 0.01–0.02, and 1–10 are 63.76, 30.95, and 62.21, respectively. Hence the resistivity range 0.001–0.005 gives the highest effective mean porosity; the Taguchi design initially optimizes the same and proceeds further to select the optimal anodization current and concentration ratio. Among the parameters affecting the porosity, resistivity is the most important, followed by anodization current and electrolyte concentration ratio (resistivity > anodization current > concentration ratio). S/N ratio decides the most affecting controlling parameter to the output parameter. However, there is no correlation between the S/N ratio and the optimal mean output parameter.

The Taguchi design predicts maximum porosity of 70.94% as it uses the mean effect of each parameter and provides the average results. Figure 5 represents the interaction graph of optimizing parameters. The interaction of anodizing current and resistivity in Fig. 5a shows anodizing current at 0.4 A, and resistivity at 1–10 Ω cm has the highest porosity, 89.11%. The interaction of anodizing current and concentration ratio in Fig. 5b shows at 0.4 A, anodizing current and concentration ratio at 3 : 7 has maximum porosity, 89.11%. However, Fig. 5c shows that resistivity at 1–10 Ω cm and concentration ratio at 2 : 3 has a maximum porosity of 75.78%. As explained above, the mean porosity calculated in the OA gives only the average porosity for each experimental sequence rather than the sufficient condition for optimization. Hence, considering all the parameters effects, the anodizing current, resistivity, and concentration ratio are at 0.4 A, 0.001–0.005 Ω cm, and 2 : 3, respectively, providing the maximum mean porosity.

Table 3 concludes the effect of four controlling parameters on the porosity, etch rate, and thickness of the PS film as reported in the literature and confirmed by the Taguchi design carried out. These four can be divided into two groups: group I parameter has a pro-

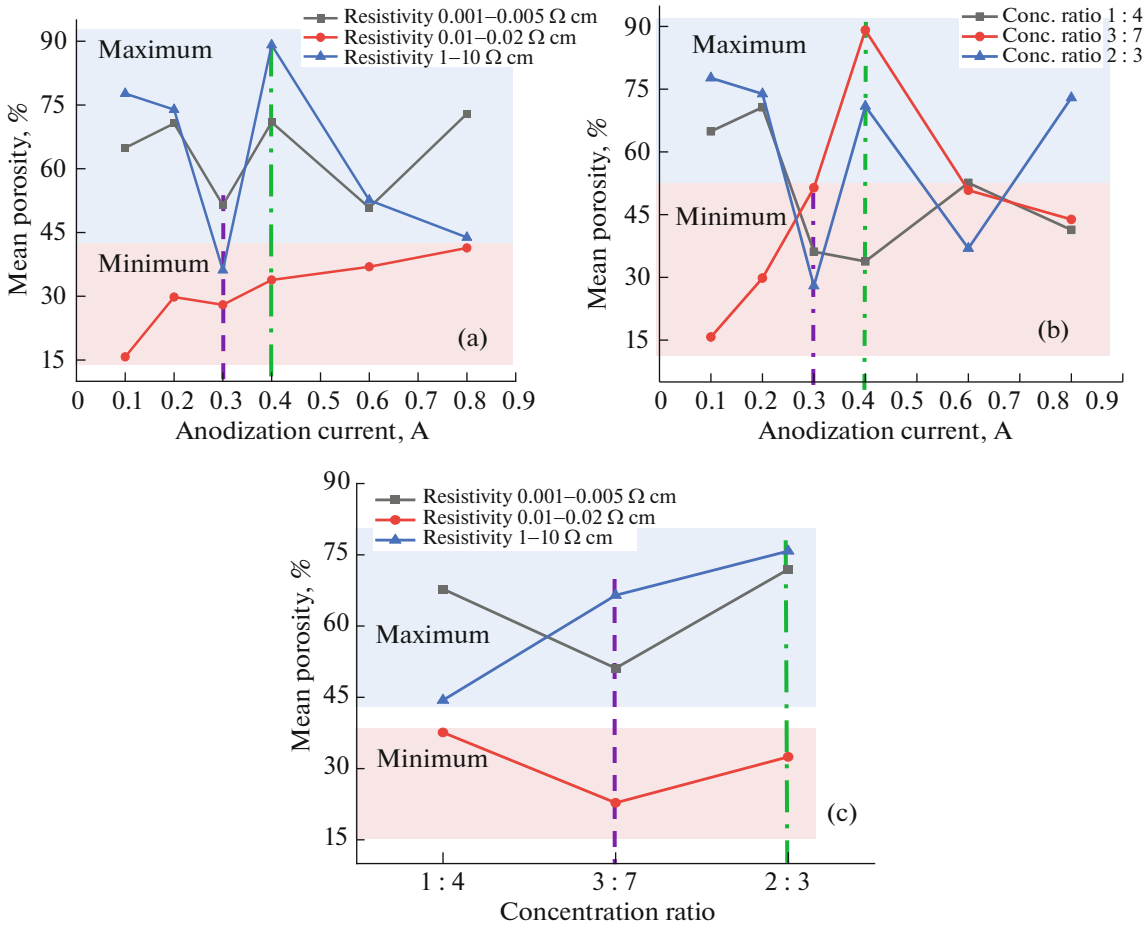

Fig. 5. The interaction graph of mean porosity with (a) current and resistivity, (b) current and electrolyte concentration ratio, and (c) electrolyte concentration ratio and resistivity.

nounced effect on the film properties as it affects the distribution of etching reaction, whereas group II parameters are less dominant, affecting the carrier density at the surface of the pores.

As per the requirements for the application of PS film, the controlling parameters may be chosen to fabricate PS films. Silicon with higher porosity is helpful for gas sensors [22] and photodetectors [23]. Although high surface area and decreased refractive index improve optical performance, increased porosity reduces mechanical strength and increases the electrical resistance of the free-standing porous film. The Low-porosity surface is preferred for storage applications such as solid-state hydrogen storage and battery anodes due to increased adsorption-desorption cycle life.

4. CONCLUSIONS

The optimization of three controlling parameters, anodizing current, resistivity, and HF to ethanol concentration ratio, was performed to optimize the porosity using the Taguchi design. The total number of the experiments was reduced by 66.7% using an orthogonal array in the case studied. The S/N ratio obtained

Table 3. Individual Parameters' effect on the porosity, etch rate, and PS film thickness

Group and its effect	Porosity parameter		Porosity	Etch rate	Thickness
I: Distribution of etching reaction	Resistivity/doping density	↑	↑	↓	↓
II: Carrier density at the surface of the pore	HF concentration	↑	↓	↓	↑
	Anodization current	↑	↑	↑	↑
	Anodization time	↑	↑	—	↑

* Where, ↑ represents increase and ↓ represents a decrease.

concludes that resistivity is the most influential parameter, followed by anodizing current and concentration ratio. Depending upon the application, Taguchi design helps to reduce the physical number of experiments to fabricate PS thin films while choosing optimized controlling parameters.

ACKNOWLEDGMENTS

The research is part of a project funded by DST-IIT Bombay Energy Storage Platform on Hydrogen (DST/TMD/MECSP/2K17/14 (G), 14-Feb-2019). The authors thankfully acknowledge the financial support extended by DST, Govt. of India.

CONFLICT OF INTEREST

The authors declare that they have no conflicts of interest.

REFERENCES

1. K. A. Salman, K. Omar, and Z. Hassan, Superlatt. Microstruct. **50**, 647 (2011).
2. A. Vu, Y. Qian, and A. Stein, Adv. Energy Mater. **2**, 1056 (2012).
3. J. H. Park, L. Gu, G. von Maltzahn, et al., Nat. Mater. **2009** (8), 331 (2009).
4. Y. Liu, T. Lai, H. Li, et al., Small **8**, 1392 (2012).
5. P. Biswas, A. K. Karn, P. Balasubramanian, and P. G. Kale, Biosens. Bioelectron. **94**, 589 (2017).
6. C. W. Jang, D. H. Shin, and S.-H. Choi, J. Alloys Compd. **877**, 160311 (2021).
7. R. Fopase, S. Paramasivam, P. Kale, and B. Paramasivan, J. Environ. Chem. Eng. **8**, 104266 (2020).
8. N. Zilony-Hanin, M. Rosenberg, M. Richman, et al., Small **15**, e1904203 (2019).
9. R. Vercauteren, G. Scheen, J.-P. Raskin, and L. A. Francis, Sens. Actuat., A **318**, 112486 (2021).
10. P. G. Kale and C. S. Solanki, in *Proceedings of the IEEE Photovoltaic Specialists Conference* (IEEE, 2010), p. 3692.
11. Y. Lai, J. R. Thompson, and M. Dasog, Chem. - Eur. J. **24**, 7913 (2018).
12. H. Jia, J. Zheng, J. Song, et al., Nano Energy **50**, 589 (2018).
13. F. Wang, L. Sun, W. Zi, et al., Chem. - Eur. J. **25**, 9071 (2019).
14. P. G. Kale, P. Sharma, and C. S. Solanki, J. Nano Res. **17**, 13 (2012).
15. E. Barsotti, S. P. Tan, S. Saraji, et al., Fuel **184**, 344 (2016).
16. M. K. Sahoo and P. Kale, Thin Solid Films **698**, 137866 (2020).
17. T. Kıvak, Measurement **50**, 19 (2014).
18. J. S. Oakland, *Total Quality Management and Operational Excellence* (Routledge, London, 2014).
19. Y.-D. Chiang, H.-Y. Lian, S.-Y. Leo, et al., J. Phys. Chem. C **115**, 13158 (2011).
20. A.-H. Chiou, W.-F. Wu, D.-Y. Chen, and C.-Y. Hsu, J. Nanopart. Res. **15**, (2013).
21. S. Song, H. B. Cho, and H. T. Kim, J. Ind. Eng. Chem. **61**, 281 (2018).
22. H. Kim, J. Yun, M. Gao, et al., ACS Appl. Mater. Interfaces **12**, 43614 (2020).
23. R. A. Ismail, A. M. Alwan, and A. S. Ahmed, Appl. Nanosci. (Switzerland) **7**, 9 (2017).